Available online at www.sciencedirect.com

SCIENCE DIRECT®

Solid State Ionics 171 (2004) 25–31

SOLID STATE IONICS

www.elsevier.com/locate/ssi

Nanostructured $LiMn_2O_4$ prepared by a glycine-nitrate process for lithium-ion batteries

Yuelan Zhang, Heon-Cheol Shin, Jian Dong, Meilin Liu*

Center for Innovative Fuel Cell and Battery Technologies, School of Materials Science and Engineering, Georgia Institute of Technology, 771 Ferst Drive, Atlanta, GA 30332-0245, USA

Received 2 December 2003; received in revised form 8 April 2004; accepted 15 April 2004

Abstract

Porous nanostructured spinel $LiMn_2O_4$ has been successfully synthesized using a glycine-nitrate combustion process. The average primary particle size of the as-synthesized powders was about 10 nm, but increased to about 100 nm with improved crystallinity after calcination at 800 °C for 2 h. Yet, the calcined powders were still highly porous and displayed reversible capacity of about 112 mA h g^{-1} at a discharge rate of 49.0 μA cm^{-2} (C/5 rate). At a high discharge rate of 2.44 mA cm^{-2} (10C rate), the obtainable reversible capacity was 57 mA h g^{-1}.

Keywords: Lithium-Ion Batteries; Glycine-nitrate Process; Nanostructure; $LiMn_2O_4$

1. Introduction

Spinel $LiMn_2O_4$ is a promising positive electrode material for rechargeable lithium-ion batteries because of its high reduction potential, low cost and acceptable environmental impact as compared to $LiCoO_2$ [1,2]. To date, a variety of dry-(solid-state) and wet-chemical techniques have been explored to control the structural and hence electrochemical properties of $LiMn_2O_4$ [3–11]. Among these, glycine-nitrate process (GNP) seems to be one of the most attractive methods, which is a self-sustaining combustion process using metal nitrates as the oxidizer and glycine as the fuel [12]. Further, the glycine plays another important role: it complexes the metal cations to prevent selective precipitation in the precursor solution. Since all constituents of the precursors can be homogeneously distributed at the molecular level in a solution, desired compositions can be readily obtained. To acquire the desired crystalline phases, a subsequent short-time annealing can be used. In contrast, the solid-state techniques and wet-chemical methods (such as sol–gel and Pechini processes) often involve a long processing time at high temperatures to form the required crystalline phases.

In particular, the vigorous gas evolution of a combustion reaction often produces highly open, nanostructured powders; the detailed microstructures of the powders, however, depends critically on the combustion parameters such as the ratio of fuel to oxidant, cation concentration to fuel and the amount and evolution rate of the gases released during a combustion process.

While a number of researchers have reported the syntheses of the intercalation compounds using the combustion process [7–11], the role of gas evolution in creating porous structures with high surface area is yet to be investigated. The nanoporous structures with the high porosity and large surface area are highly desirable for electrode applications in solid state electrochemical systems. In this communication, we report the structural and electrochemical properties of highly open nanostructured $LiMn_2O_4$ with spinel structure prepared by a modified glycine-nitrate process.

2. Experimental

2.1. Powder preparation

Stoichiometric amounts of $LiNO_3$ and $Mn(CH_3COO)_2 \cdot 4H_2O$ were dissolved in distilled water. Nitric acid with the same mole of acetate anions was added to the solution. The molar ratio of glycine to nitrate was one. The resulting

* Corresponding author. Tel.: +1-404-894-6114; fax: +1-404-894-9140.
E-mail address: meilin.liu@mse.gatech.edu (M. Liu).

0167-2738/$ - see front matter © 2004 Elsevier B.V. All rights reserved.
doi:10.1016/j.ssi.2004.04.008

solution was heated on a hot plate to evaporate the excess solvent, producing the viscous resin and then dark brownish foam. When further heated, it ignited, yielding a voluminous, black, sponge-like ash. The resulting ash was subsequently fired in air at 800 °C for 2 h. In particular, the precursor $Mn(CH_3COO)_2{\cdot}4H_2O$ was chosen instead of $Mn(NO_3)_2{\cdot}xH_2O$ because it produces a greater amount of gas during combustion, which is favorable to producing highly open porous microstructures and, at the same time, it obviates the ambiguity of the amount of crystalline water in the manganese salt.

For the sake of comparison, spinel $LiMn_2O_4$ was also fabricated using a conventional solid-state reaction. $LiMn_2O_4$ powder was prepared by heating a pressed mixture of stoichiometric amounts of $LiNO_3$ and Mn_2O_3 at 850 °C for 48 h in air with intermittent grindings, followed by a ball-milling for 24 h. The average particle size of the resulting powder was about 5 μm as estimated from an SEM (Hitachi S-800 Scanning Electron Microscope) observations.

2.2. Characterization

X-ray powder diffraction (XRD) patterns were recorded with Philips PW-1800 X-ray Diffractometry (with CuKα radiation). The chemical compositions of the samples were analyzed using an inductively coupled plasma (ICP) technique (PerkinElmer Optima 3000DV) to estimate the ratio of Mn to Li. The morphology was revealed using an SEM and a TEM (Hitachi HF-2000 Transmission Electron Microscope). The specific surface area was measured by the Brunauer-Emmett-Teller (BET) method (Micromeretics ASAP 2000).

The tapping density of the powders was roughly estimated by placing a known mass of the powder (500 mg) in a glass tube (0.5 cm diameter) and tapping it 300 times on a lab bench. The density of the powder exhibited a slow relaxation approach to the final packing state, i.e. after 300 tappings the density (or volume) of the powder showed little change with the number of tapping, which was taken as the tapping density of the powder.

Two-electrode electrochemical cells were employed for electrochemical measurements using lithium foils as the counter and reference electrode. The working electrode was composed of calcined $LiMn_2O_4$ (78 wt.%), carbon black (10 wt.%) and polyvinylidene fluoride (PVDF) binder (12 wt.%). The mixture was prepared by ball milling and the slurry was cast on Al foil, followed by drying at 180 °C in vacuum for 24 h and uniaxial pressing between two flat plates at ~ 500 psi for 5 min. The electrode loading was 2.04 mg of spinel $LiMn_2O_4$ in a square centimeter of Al. A Celgard 2400 separator, wetted with 1 M solution of $LiPF_6$ in a 50/50 (v/o) mixture of ethylene carbonate (EC) and diethyl carbonate (DEC), was sandwiched between an $LiMn_2O_4$ working electrode and a lithium counter electrode. All cells were assembled and tested in a glove box (Vacuum Atmospheres Company) filled with purified argon gas. A Solartron 1285 potentiostat was employed to carry out the cyclic voltammetry, chronoamperometry and galvanostatic intermittent titration technique (GITT). And a Maccor battery test system (Model 2300) was used to evaluate the rate capability and cyclability.

In particular, for the rate capability test, a charging current of 61.2 μA cm^{-2} (C/4 rate; a nominal specific capacity of 120 mA h g^{-1} was assumed to convert the current density into C rate) was applied until the cell voltage reached 4.4 V (vs. Li/Li^+). Subsequently, discharging currents in the range of 61.2 μA cm^{-2} (C/4) to 4.90 mA cm^{-2} (20C) were applied until the cell voltage reached 3.3 V (vs. Li/Li^+). A GITT was employed to estimate the chemical diffusion coefficient of lithium in the solid state [13]. In a typical measurement, a constant current of 50 μA cm^{-2} was applied to the cell for 1000 s, and then was interrupted for 2000 s to allow the cell to equilibrate. The voltage profile during current application/interruption was recorded and the voltage at the end of current interruption was taken as the open circuit voltage. The current application/interruption was repeated until the (closed circuit) potential reached 3.0 (V vs. Li/Li^+). The degree of discharge (DOD) or lithium content $1-\delta$ in $Li_{1-\delta}Mn_2O_4$ was estimated from the mass of the oxide and the charge transferred during current application.

3. Results and discussion

Shown in Fig. 1 are the X-ray diffraction patterns of as-synthesized and calcined powders. It is clear that there exist Mn_3O_4 and Mn_2O_3 phases with lower valence state of Mn than $LiMn_2O_4$ in the as-synthesized powder along with some unidentified phases, probably the distorted $LiMn_2O_4$. After calcination in air at 800 °C for 2 h, however, crystalline spinel structure of $LiMn_2O_4$ was formed. From the Rietveld refinement method, the lattice parameter of our spinel $LiMn_2O_4$ was calculated to be 8.237 Å. Moreover, The ICP analysis showed that the atomic ratio of Mn to Li is 2.04. Both lattice parameter and atomic ratio of Mn to Li for our $LiMn_2O_4$ are similar to those reported in the literature for the conventional stoichiometric $LiMn_2O_4$ [8,11]. The tapping density of our powder was about 0.72 g cm^{-3}, which is much smaller than a typical value of 2.5–3.0 g cm^{-3} for the commercially available positive electrodes, probably due to the highly porous feature of our powder. The adjustment of the (micro-)structure of the GNP-prepared powder, including the size distribution of the pore as well as the fragmented particles after mechanical grinding, is expected to increase the tapping density of the powder.

Shown in Fig. 2 are some typical TEM images of the as-synthesized and calcined $LiMn_2O_4$ powders. The primary particle size of the as-synthesized powders (Fig. 2(a)) is around 10 nm with visible agglomerations. The average

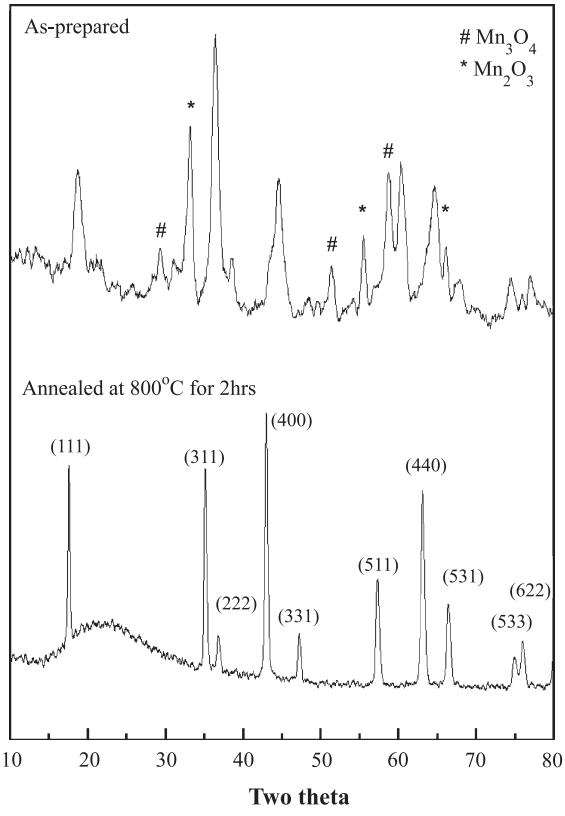

Fig. 1. X-ray diffractograms of as-synthesized and calcined $LiMn_2O_4$ powders at 800 °C for 2 h.

particle size increased to about 100 nm after firing at 800 °C for 2 h, as shown in Fig. 2(b). Fig. 3 depicts the typical morphologies of calcined powders which are characteristic of a macroporous structure with uniformly distributed interconnected pores of about 500 nm in diameter. The as-synthesized and calcined powders typically have surface areas of 17.0 and 5.9 $m^2\ g^{-1}$, respectively, as measured by the BET technique. Based on the BET results, the equivalent particle sizes of the as-synthesized and calcined powders were estimated to be 82 and 236 nm, respectively, assuming that the particles are spherical and there is no contact among the particles. The calculated particle sizes match satisfactorily the observed particle sizes from TEM, in spite of the possible overestimation of the calculated particle sizes due to the roughness of the particle (Fig. 2) and interconnection between the particles (Fig. 3). This high porosity of the $LiMn_2O_4$ is attributed to the vigorous gas evolution (H_2O, N_2 and CO_2) during the combustion synthesis.

$$2Mn(CH_3COO)_2 \cdot 4H_2O + 4HNO_3 + LiNO_3 + 2NH_2CH_2COOH \xrightarrow{\text{combustion in air}} LiMn_2O_4 + 17H_2O\uparrow + (7/2)N_2\uparrow + 12CO_2\uparrow$$

This microstructural and morphological disturbance/distortion are expected to facilitate mass and charge transport through the porous electrodes during lithium battery operation [14–16].

Lithium insertion (discharge)/extraction (charge) reaction into/from spinel $LiMn_2O_4$ proceeds reversibly according to the following equation [17].

$$Li_xMn_2O_4 + \Delta x Li^+ + \Delta x e^- \underset{\text{charge (lithium extraction)}}{\overset{\text{discharge (lithium insertion)}}{\rightleftharpoons}} Li_{x+\Delta x}Mn_2O_4$$

In order to evaluate the properties of the GNP-prepared $LiMn_2O_4$ powder during the electrochemical lithium insertion/extraction, a variety of electrochemical testing were performed. Shown in Fig. 4(a) is a typical cyclic voltammogram of the calcined powder at a scan rate of 0.1 mV/s. Two anodic peaks at 4.08 and 4.22 V (vs. Li/Li^+) and the corresponding two cathodic peaks at 3.93 and 4.05 V (vs. Li/Li^+) are ascribed to the lithium extraction and insertion processes, respectively. Shown in Fig. 4(b) is a typical galvanostatic charge/discharge profile of the calcined powders at a current density of 49.0 μA cm^{-2} (C/5 rate), showing a two-staged lithium insertion/deinsertion behavior, consistent with the cyclic voltametry result. The two quasi-potential plateaus are a characteristic of a well-defined $LiMn_2O_4$ spinel [1,2]. The specific reversible capacity is about 112 mA h g^{-1} (228 μA h cm^{-2}) during both charging

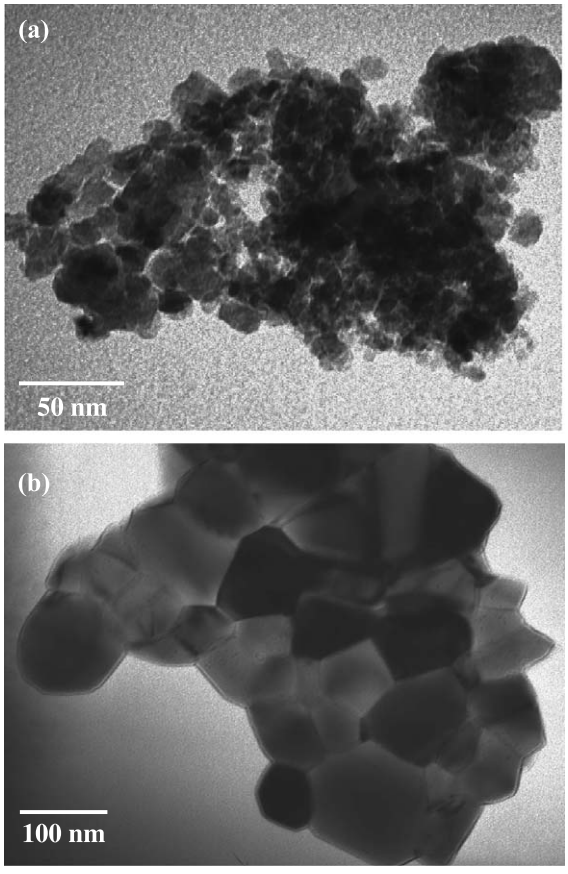

Fig. 2. TEM images of (a) as-synthesized and (b) calcined powders.

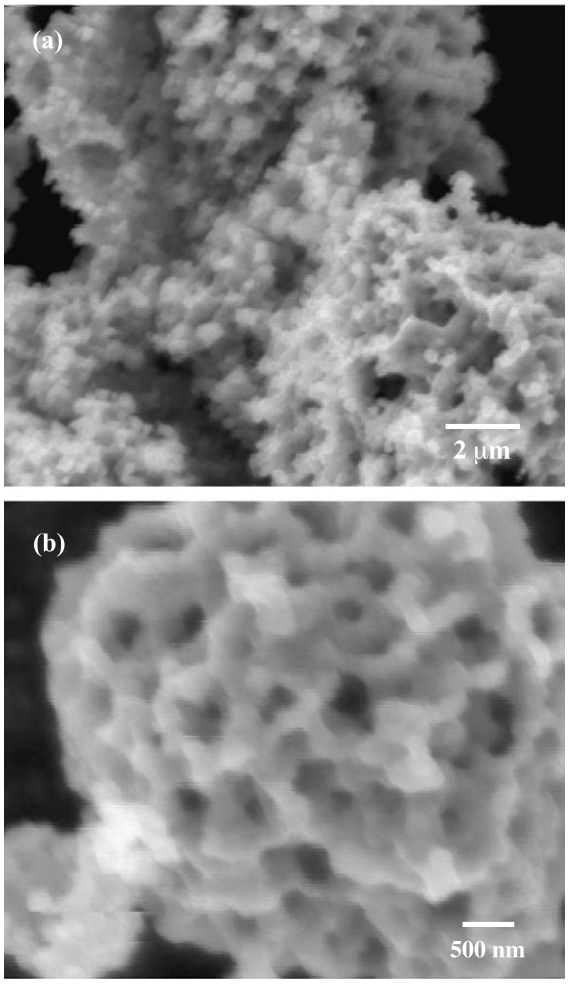

Fig. 3. SEM images of calcined powders at (a) low and (b) high magnifications.

and discharging processes, implying reversible lithiation/delithiation of the calcined $LiMn_2O_4$ powders.

The theoretical specific capacity of $LiMn_2O_4$ is 148 mA h g^{-1} when lithium is fully extracted to form λ-MnO_2. The discrepancy between the theoretical and experimental specific capacities is due probably to kinetic limitation of the lithium extraction reaction at relative fast lithium extraction process as well as the difficulty in full electrochemical extraction of lithium to form λ-MnO_2 at practical potential (< 5 V vs. Li/Li^+) [17]. When we consider the mass of binder (12 wt.%) and current collector (10 wt.%), the theoretical and experimental capacities per unit mass of the composite electrode become 115.4 and 87.4 mA h g^{-1}, respectively. On the other hand, the theoretical capacity density (volumetric) of the ideally dense $LiMn_2O_4$ is known to be 634 mA h cm^{-3} [17] while the experimental capacity density of our GNP-prepared $LiMn_2O_4$ porous composite (including additives such as binder and carbon) was estimated to be 120 mA h cm^{-3}. The much smaller capacity density of our powder than pure dense $LiMn_2O_4$ is attributed to the large amount of additives as well as the porous feature of our powder and a pressed composite electrode.

The rate capability of the same powders during discharging processes is shown in Fig. 5. At discharging rates of C/4 (61.2 μA cm^{-2}), C/2 (122.4), 1C (244.8), 2C (489.6), 3C (734.4), 5C (1224) and 10C (2448), the cell delivered specific capacities of 108 (220), 104 (212), 102 (208), 89 (182), 83 (169), 76 (155) and 57 mA h g^{-1} (116 μA h cm^{-2}), respectively. In particular, more than 50% of the reversible capacity at C/4 rate can be discharged at 10C rate. This rate capability is higher than the rate capability for the spinel $LiMn_2O_4$ prepared by a conventional solid-state reaction, as shown in Fig. 5(b), as well as those reported for the spinels fabricated by the similar solid-state reactions [18,19], but smaller than those for the spinels created by

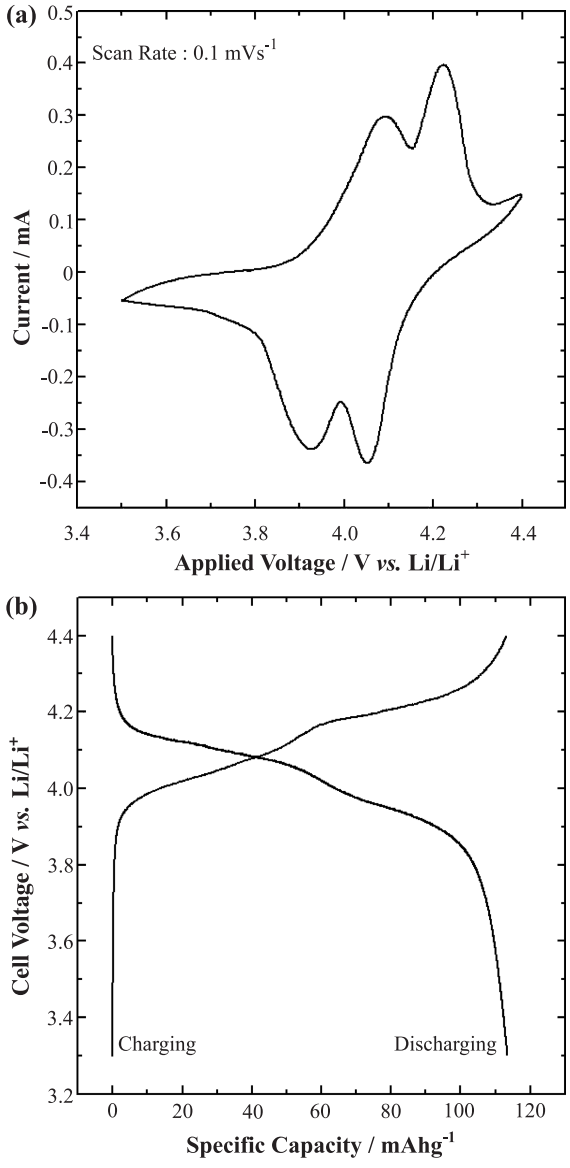

Fig. 4. (a) Typical cyclic voltammogram of calcined powders at the scan rate of 0.1 mV/s and (b) galvanostatic charge/discharge curve at the current density of 49.0 μA cm^{-2} (C/5 rate).

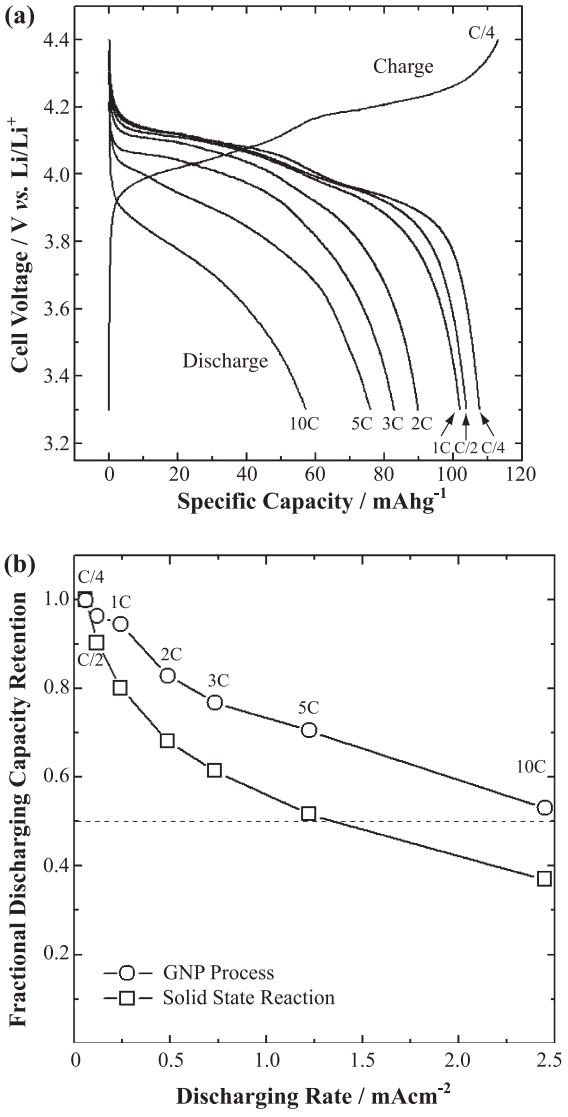

Fig. 5. (a) Dependence of voltage profile on applied current density and (b) variation of fractional discharging capacity retention in discharging rate (open circle), reconstructed from Fig. 5(a). For the sake of comparison, the discharging capacity retention of the $LiMn_2O_4$ prepared by a conventional solid-state reaction was included (open square). The specific discharge capacities at C/4 rate of two samples prepared by GNP and solid-state reaction were 108 and 112 mA h/g, respectively.

sophisticated techniques such as a template method [20] and spray-drying process [21]. Nevertheless, the combustion process has a great potential to create a variety of morphologies with different rate capacities because the rate capability depends critically on the electrochemically active surface area and/or pore size of the powders. In this combustion process, the surface area and porosity of the powders are critically affected by the ratio of the precursor to fuel, which determines the rate of gas evolution during the combustion process.

Shown in Fig. 6 is the cycling behavior of the calcined powder at a current density of 122.4 μA cm^{-2} (C/2 rate). The discharging capacity retention was about 90% at the

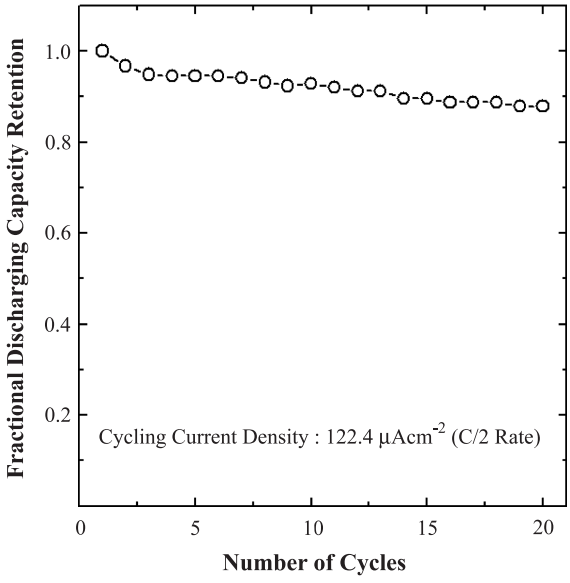

Fig. 6. Dependence of discharging capacity retention of calcined powders on the number of cycles at the cycling rate of 122.4 μA cm^{-2} (C/2).

20th cycle and half of the capacity loss occurred during the first several cycles. This relatively large capacity fade is typical for the spinel $LiMn_2O_4$, making it impractical for real applications. Nevertheless, recent work has shown that the cyclability can be significantly improved by introducing dopants to the $LiMn_2O_4$ [22,23]. The effects of dopants on long-term cycling performance of GNP-prepared powders are still under investigation.

In order to explore the kinetics of lithium transport through the electrode materials, chronoamperometry was performed between 3.9 and 4.2 V (vs. Li/Li^+). Shown in Fig. 7 are the $I{\cdot}t^{1/2}$ vs. log t plots; however, there is no plateau region (i.e. no Cottrell region) throughout the intercalation/deintercalation time, indicating that the overall process was not controlled by lithium diffusion (e.g., the interfacial resistance could be significant as compared to diffusional resistance [24]). This further implies that the lithium transport through the calcined $LiMn_2O_4$ electrode is

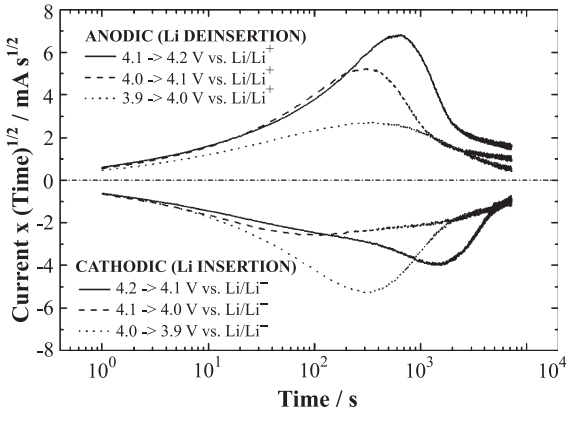

Fig. 7. Typical chronoamperometric curves of calcined powders.

possibly controlled by slow interfacial reaction during the chronoamperometric measurement [24,25]. Under the circumstances, it is unlikely that the analysis of the chronoamperometric curves gives us reliable values of diffusion coefficient. Instead, we adopted a GITT to evaluate the diffusion coefficient.

Shown in Fig. 8(a) is a typical voltage transient during a current application and a subsequent current interruption in the GITT experiment. In a very short time range, where semi-infinite lithium diffusion in the solid state occurs, the cell voltage is proportional to the square root of time, as suggested by a linear regression analysis (insert in Fig. 8(a)). From the potential transient (e.g. insert in Fig. 8(a)) and the coulometric titration curve (Fig. 8(b)), the chemical diffusion coefficient of lithium was determined as a function of lithium content $(1-\delta)$ [13]. The value of diffusion coefficient ranged from 10^{-10} to 10^{-13} cm^2/s. In particular, the dependence of the diffusion coefficient on $(1-\delta)$ shows two minima in the $(1-\delta)$ regions where quasi-potential plateaus are observed, which are attributed to

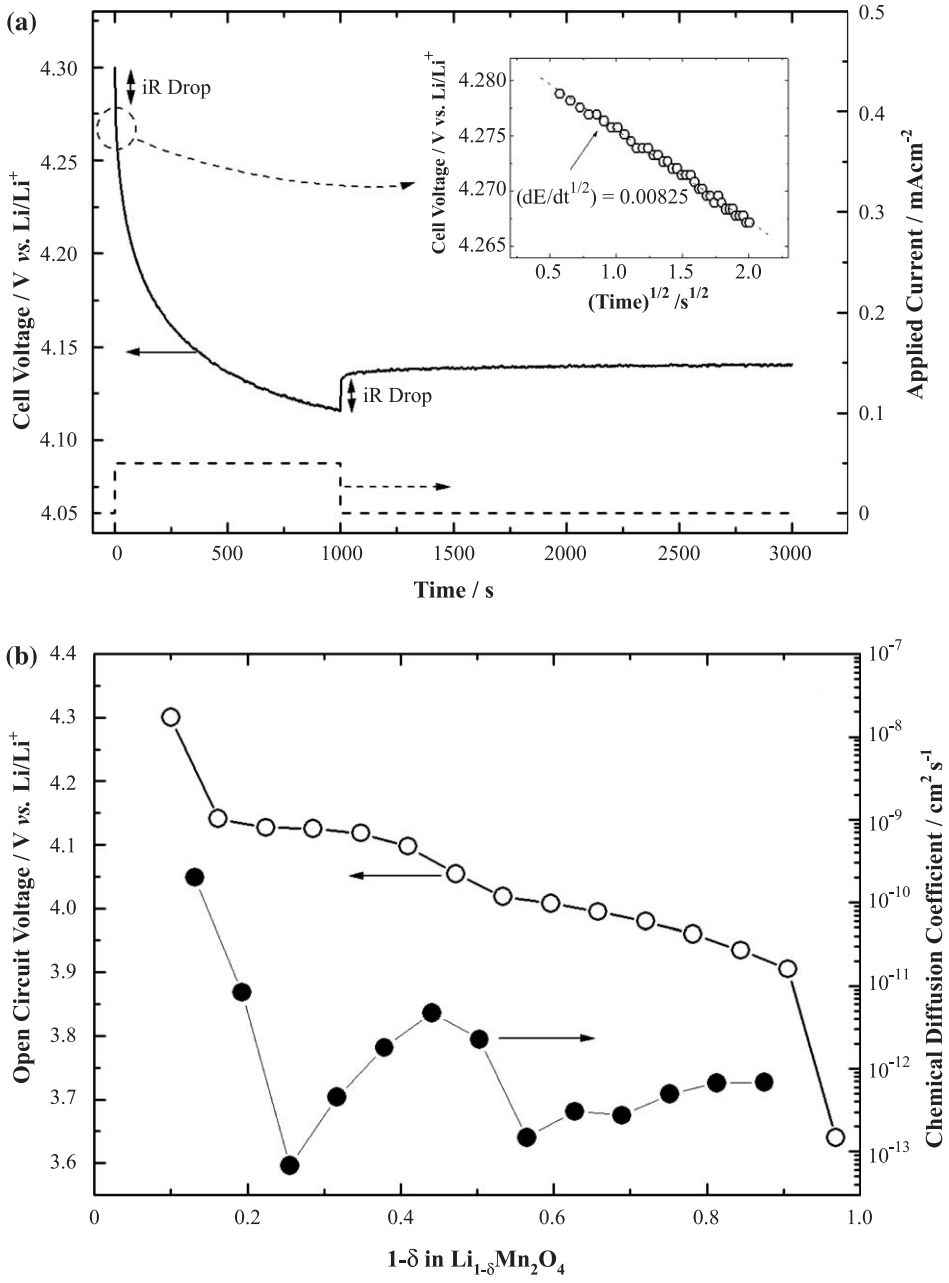

Fig. 8. (a) Typical voltage transient during a current application and a subsequent current interruption in the GITT experiment and cell voltage (V) vs. time$^{1/2}$ ($t^{1/2}$) plot in a very short time range (insert in Fig. 8(a)) showing the linear relationship between V and $t^{1/2}$, and (b) open circuit voltage obtained from the GITT experiment (open circle) and chemical diffusion coefficient (solid circle) as a function of lithium content.

high attractive interactions related to lithium intercalation process [26].

4. Conclusion

Nanostructured $LiMn_2O_4$ spinel has been successfully synthesized using a glycine-nitrate combustion process followed by a short-time calcination. The calcined powder retained a porous nanostructure but with improved crystallinity and showed quite reversible lithiation and delithiation during cycling. The obtainable reversible capacity of the calcined powder was about 112 mA h g^{-1}. In particular, more than 50% of the reversible capacity (57 mA h g^{-1}) could be delivered at a high discharge rate of 2.44 mA cm^{-2} (10C), which is a higher rate capability than those reported for the spinel $LiMn_2O_4$ prepared by conventional solid-state reactions. The glycine-nitrate process appears to be an attractive method for fabrication of cost-effective nanostructured electrodes for lithium secondary batteries.

Acknowledgements

This work was supported by the Office of Science, Department of Energy under Grant No. DE-FG02-01ER15220.

References

[1] J.M. Tarascon, D. Guyomard, J. Electrochem. Soc. 138 (1991) 2864.
[2] D. Guyomard, J.M. Tarascon, J. Electrochem. Soc. 139 (1992) 937.
[3] J.C. Hunter, J. Solid State Chem. 39 (1981) 142.
[4] J.M. Tarascon, W.R. McKinnon, F. Coowar, T.N. Bowmer, G. Amatucci, J. Electrochem. Soc. 141 (1994) 1421.
[5] W. Liu, G.C. Farrington, F. Chaput, B. Dunn, J. Electrochem. Soc. 143 (1996) 879.
[6] Z. Zian, K.M. Abraham, J. Electrochem. Soc. 143 (1996) 1591.
[7] J. Guan, M.L. Liu, in: P.N. Kumta, G.S. Rohrer, U. Balachandran (Eds.), Role of Ceramics in Advanced Electrochemical Systems, Ceramic Transactions, vol. 65, The American Ceramic Society, Westerville, OH, 1997, p. 149.
[8] H.-B. Park, J.-S. Kim, C.-W. Lee, J. Power Sources 92 (2001) 124.
[9] E.I. Santiago, S.T. Amancio-Filho, P.R. Bueno, L.O.S. Bulhoes, J. Power Sources 97–98 (2001) 447.
[10] S. Rodrigues, N. Munichandraiah, A.K. Shukla, J. Power Sources 102 (2001) 322.
[11] K. Du, H. Zhang, J. Alloys Compd. 352 (2003) 250.
[12] L.A. Chick, L.R. Pederson, G.D. Maupin, J.L. Bates, L.E. Thomas, G.J. Exarhos, Mater. Lett. 10 (1990) 6.
[13] W. Weppner, R.A. Huggins, J. Electrochem. Soc. 124 (1977) 1569.
[14] T.D. Tran, J.H. Feikert, R.W. Pekala, K. Knoshita, J. Appl. Electrochem. 26 (1996) 1161.
[15] G.S. Nagarajan, J.W. Van Zee, R.W. Sptnitz, J. Electrochem. Soc. 145 (1998) 771.
[16] F. Coustier, J. Hill, B.B. Owens, S. Passerini, W.H. Smyrl, J. Electrochem. Soc. 146 (1999) 1355.
[17] M. Winter, J.O. Besenhard, M.E. Spahr, P. Novak, Adv. Mater. 10 (1998) 725.
[18] D.I. Siapkas, C.L. Mitsas, I. Samaras, T.T. Zorba, G. Moumouzias, D. Terzidis, E. Hatzikraniotis, S. Kokkou, A. Voulgaropoulos, K. M. Paraskevopoulos, J. Power Sources 72 (1998) 22.
[19] Z. Liu, A. Yu, J.Y. Lee, J. Power Sources 74 (1998) 228.
[20] N. Li, C.J. Patrissi, G. Che, C.R. Martin, J. Electrochem. Soc. 147 (2000) 2044.
[21] M. Lanz, C. Kormann, H. Steininger, G. Heil, O. Haas, P. Novak, J. Electrochem. Soc. 147 (2000) 3997.
[22] L. Guohua, H. Ikuta, T. Uchida, M. Wakihara, J. Electrochem. Soc. 143 (1996) 178.
[23] A.D. Robertson, S.H. Lu, W.F. Averill, W.F. Howard Jr., J. Electrochem. Soc. 144 (1997) 3500.
[24] C. Montella, J. Electroanal. Chem. 518 (2002) 61.
[25] H.-C. Shin, S.-I. Pyun, in: R.E. White, B.E. Conway, C.G. Vayenas (Eds.), Modern Aspects of Electrochemistry, vol. 36, Plenum, New York, 2002, p. 255.
[26] M.D. Levi, K. Gamolsky, D. Aurbach, U. Heider, R. Oesten, J. Electrochem. Soc. 147 (2000) 25.